Effect of pressure on atomic volume and crystal structure of indium to 67 GPa

Olaf Schulte and Wilfried B. Holzapfel
Fachbereich Physik, Universität Paderborn, D 33095 Paderborn, Germany
(Received 10 December 1992; revised manuscript received 16 February 1993)

The crystal structure of indium is studied by energy-dispersive x-ray diffraction with diamond anvil cells at ambient temperature under pressures up to 67 GPa. The present results are compared with previous volumetric data for the lower-pressure region as well as with data from shock-wave measurements extending to higher pressures. A comparison of these data with different forms representing equations of state for solids under strong compression shows that indium can be classified as a "simple" solid. No structural phase transitions are observed in the present experimental range up to 67 GPa.

I. INTRODUCTION

The development of diamond anvil cells for the generation of pressures in the range to 100 GPa,[1] together with suitable x-ray-diffraction techniques,[2] allows for the determination of structural parameters including equations of state (EOS) on solids under strong compression, which were previously only accessible in shock-wave compressions with all the limitations inherent in that technique.[3] A critical analysis of various EOS forms commonly used for the representation of experimental data extending into the region of strong compression has shown[4] that one specific series expansion allows not only for simple interpolations to very strong compression but results also in a classification of EOS forms representing "ideal," "simple," or more complex solids.[5] In addition, a detailed analysis of the crystal structure of indium to pressures above 50 GPa was stimulated by recent results of Takemura,[6] which gave some evidence for the beginning of a phase transition at pressures of about 44 GPa.

II. EXPERIMENTAL TECHNIQUE

A diamond anvil cell of Syassen-Holzapfel type[7,8] was used with diamonds either in the standard form (600-μm flat diameter) or beveled with 300-μm inner flat diameter. Preindented inconnel gaskets (X750) with sample areas of 180- or 100-μm diameter, respectively, were loaded with the indium samples of 99.9% purity, with a ruby sphere of typically 5-μm diameter and with either liquid nitrogen or mineral oil as pressure transmitting fluid. The pressure was determined with the ruby luminescence technique[9] and the use of the nonlinear pressure scale.[10] Energy-dispersive x-ray (EDX)-diffraction patterns were taken either with a conventionell 2-kW tungsten tube and the conical slit system[11] or with synchrotron radiation (SR) at the energy-dispersive spectroscopy (EDS) station in HASYLAB, DESY, also previously described.[12]

III. RESULTS

Typical EDX patterns of indium at two different pressures taken at HASYLAB are shown in Fig. 1. While the pattern at 43.3 GPa was measured in 1500 s, a counting time of 5000 s was used for the pattern at 63.8 GPa. Since all the peaks can be indexed with respect to either K_α and K_β fluorescence of indium, or to escape peaks (e) from the Ge detector, or diffraction lines either from the gasket (g) or from indium in its body-centered-tetragonal (bct) structure with the given hkl values, no indication can be found for the occurrence of any contribution from any other phase or any other material even at the highest pressure, with no support of the previous observations[6] about a possible phase transition of indium around 44 GPa. Also a careful analysis of the linewidth of the diffraction peaks shows only the normal slight increase

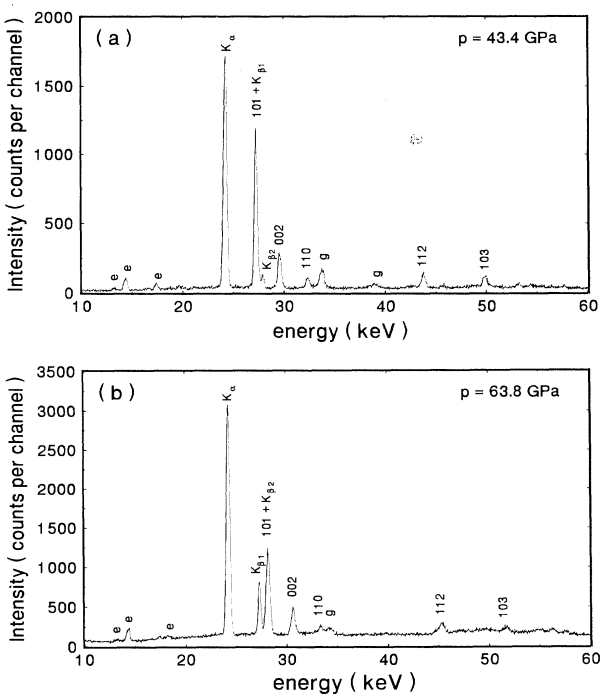

FIG. 1. EDX diffraction pattern of indium at 43.4 and 63.8 GPa with indexing for the bct structure. The lines labeled with g, K, and e refer to gasket, fluorescence, and escape peaks, respectively.

with pressure and no anomalies. A detailed evaluation of 55 EDX patterns, including the data of Ref. 13 with 47 patterns taken on increasing pressure and 8 on pressure release, results in the systematic variation of eight different lattice spacings d_{hkl} for the bct structure of indium as illustrated in Fig. 2. Best fits of the lattice parameters a and c to these data are shown in Fig. 3, where the size of the dots represents the standard deviations in the fits of typically 0.1% for both a and c. Effects from slight nonhydrostatic stresses and pressure gradients between the ruby pressure sensor and the center of the indium sample may thus account for most of the scatter in these data. No systematic differences are observed in preparations with the different pressure transmitting media used in different experiments.

With the values $a_0=0.325\,20(6)$ nm and $c_0=0.4947(1)$ nm from the literature[14] for the lattice parameters at ambient pressure and temperature and with the normalized values $x_a=a/a_0$ or $x_c=c/c_0$, respectively, one can use the analytic form of an EOS for strong compression previously discussed for isotropic solids[15] also for the representation of the pressure dependence of the lattice parameters a and c by the form

$$p=3K_{i0}x_i^{-5}(1-x_i)\exp[C_{i0}(1-x_i)]\ ,$$

with the two free parameters K_{i0} and C_{i0} for $i=a$ or c. The least-squares fitting of this form with minimization of the deviations in x_i at the given values of p results in the continuous lines included in Fig. 3, which correspond to the parameter values $K_{a0}=90(18)$ GPa, $C_{a0}=25(5)$, and $K_{c0}=153(17)$ GPa, $C_{c0}=18(5)$ whereby the statistical errors in parentheses do not include the mutual uncertainty due to the correlations in these parameters in the fitting procedure. The ratio $K_{c0}/K_{a0}=1.7(4)>1$ shows that the compression of indium at low pressures is slightly anisotropic, and the ratio $C_{c0}/C_{a0}=0.4(2)<1$ indicates that this anisotropy decreases under pressure.

This fact is illustrated more clearly in Fig. 4, where the data points are evaluated from the data in Fig. 3 with $V=a^2c/2$ for the atomic volume of indium in its bct structure and $V_0=0.026\,15(1)$ nm^3 from the literature

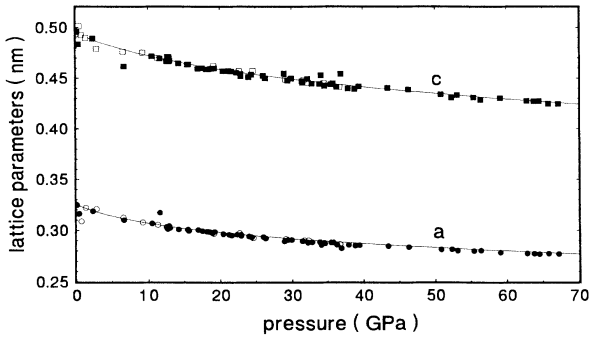

FIG. 3. Effect of pressure on the lattice parameters of indium derived from the data in Fig. 2.

values.[14] As one can see from this Fig. 4, the present data correspond to a slight increase of c/a in the initial range of weak compression ($V/V_0\geq 0.9$) with a saturation of $c/a\rightarrow 1.54$ at strong compression ($V/V_0\leq 0.7$). The few data points of the present measurements in the range $0.8<V/V_0<1$ do not allow us to draw any further conclusions on the existence of a maximum in c/a previously observed in a detailed x-ray study on indium just in this pressure region,[17] however, the present data as well as the recent data also covering an extended pressure range (up to 56 GPa) (Ref. 6) fit better to a smooth increase in c/a only. For comparison with a possible face-centered-tetragonal (fct) indexing of this body-centered-tetragonal (bct) structure, the corresponding scale for $(c/a)_{\rm fct}$ is given in Fig. 4 on the right-hand side. This scale may show more directly that the initial slight (8%) distortion with respect to a more symmetric fcc structure increases further (slightly) and stabilizes under strong compression without any sign to approach either the ideal value for a fcc or bcc structure.

A detailed comparison of the present EOS data with previous results from the literature[3,6,16–17,19] is given in Fig. 5. A close agreement can be noticed with the recent x-ray data by Takemura[6] in the range to 56 GPa as well as with the data from the AIP *Handbook*.[3] These later results were derived from shock-wave data by correcting

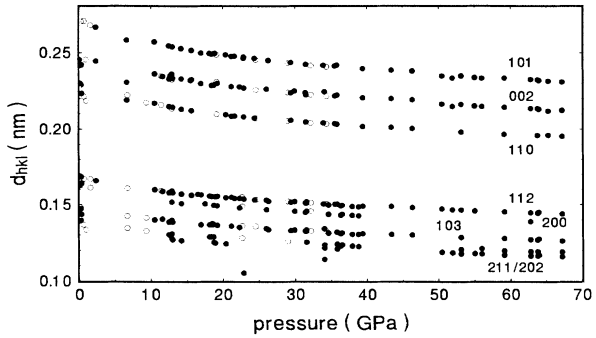

FIG. 2. Effect of pressure on lattice spacings d_{hkl} of indium with indexing for the bct structure at ambient temperature. Data for upstroke and downstroke experiments are represented by full and open circles, respectively.

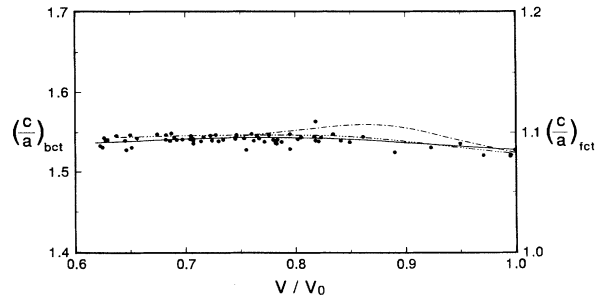

FIG. 4. Variation of c/a ratio vs relative volume V/V_0 with additional data from the literature represented by dash-dotted (Ref. 17) and dash-triple dotted (Ref. 6) lines, respectively. The continuous line illustrates the present best fit by the analytic form given in the text.

for the thermal pressure in these measurements and, thus, the close agreement between the present static isothermal measurements with these data shows that the assumptions made in these previous data reductions were indeed very reasonable. Slight deviations of the early volumetric data[18] to lower pressures as well as for the first x-ray data[17] towards higher pressures can be noticed. A more detailed comparison of these different data can be made, however, if one looks at the parameters extracted by fitting specific analytic EOS forms to these data as shown in Table I. Since the specific values derived for these parameters depend also on the specific EOS form used in the fitting of the data, a close look at the effect from different analytic EOS forms seems to be necessary at this point.

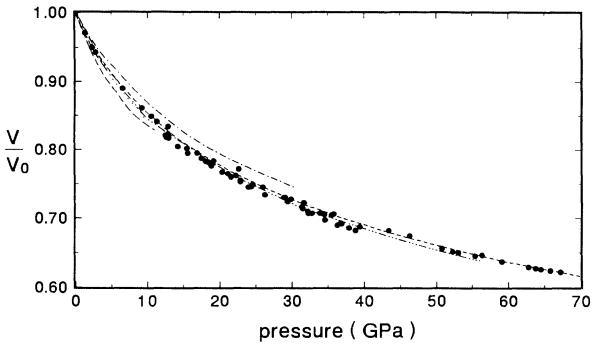

FIG. 5. Effect of pressure on relative volume V/V_0 at ambient temperature. Present data are scaled with $V_0=0.026\,15$ nm^3 for ambient pressure and temperature from the literature (Ref. 14). Previous EOS data from static measurements are represented by dotted (Ref. 16), dash-dotted (Ref. 17) and dash-triple dotted (Ref. 6) lines and results from shock-wave measurements (Ref. 3) by the dashed line, respectively.

IV. DISCUSSION

Since the present data for indium cover a wide range in compression ($0.6 \leq V/V_0 \leq 1$) without any indication of anomalies or structural phase transitions, Fig. 5, these

TABLE I. Numerical results for fits of different EOS data sets with different EOS forms. The names for the EOS forms are explained in the text. Isothermal values derived from ultrasonic measurements are included for comparison in the last section marked as US.

K_0 (GPa)	K_0'	p_m (GPa)	σ_V (%)	$-\epsilon$	EOS	Ref.
41(2)	4.5(2)	67	0.790	0.976	MU2	
38(2)	5.5(3)	67	0.713	0.983	BE2	Fit of
36(2)	6.0(3)	67	0.686	0.982	MV2	present
37(2)	5.8(3)	67	0.698	0.982	H02	data
37(2)	5.8(3)	67	0.696	0.985	H12	
39	4.6(2)	67	0.804		MU2	Fit of
39	5.3(3)	67	0.727		BE2	present
39	5.6(3)	67	0.734		MV2	data
39	5.4(3)	67	0.728		H02	with K_0
39	5.4(3)	67	0.727		H12	fixed
42(3)	4.0(9)	10	0.029	0.979		16
52(2)	4.5(5)	26	0.048	0.975		17
30(4)	7(2)	11	0.658	0.985	H12	18
39(1)	5.6(9)	5	0.008	0.977		19
41(1)	5.1(2)	56	0.086	0.984		6
37(2)	5.6(3)	90	0.043	0.997		3
41(3)	4.4(3)	90	0.624	0.936	MU2	
38(3)	5.3(5)	90	0.542	0.954	BE2	Fit of
37(3)	5.8(5)	90	0.516	0.949	MV2	all
38(3)	5.6(5)	90	0.525	0.949	H02	data
38(3)	5.6(6)	90	0.527	0.955	H12	
37(3)	5.7(2)	90	0.541		H11	All
39	5.7	90	0.759			data
39(1)					US	24
40.3(8)	6.2(1)	2				25

data can serve very reasonably for a detailed comparison of different analytical EOS forms, which are either commonly used or just recently proposed specifically for solids under strong compression.[4,15] The commonly used EOS forms[20–22] are denoted here, respectively, by

$$\text{MU2: } p=\frac{3}{C_2}K_0x^{-C_2}(1-x^{C_2}), \text{ with } C_2=3K_0' ,$$

$$\text{BE2: } p=\tfrac{3}{2}K_0x^{-7}(1-x^2)[1+C_2(x^{-2}-1)] ,$$
$$\text{with } C_2=\tfrac{3}{4}(K_0'-4) ,$$

$$\text{MV2: } p=3K_0x^{-2}(1-x)\exp[C_2(1-x)] ,$$
$$\text{with } C_2=\tfrac{3}{2}(K_0'-1) ,$$

with $x=(V/V_0)^{1/3}$. K_0 represents the bulk modulus at ambient pressure, and the different parameters C_2 are related to the pressure derivative K_0' by different well-known relations also given here. These three EOS forms were derived by different approaches, however, only for the representation of EOS data of solids under moderate compression and therefore suffer from the fact that they diverge (in different directions) from the expected behavior of "regular" solids under very strong compression.[4] Thus, we arrive at the question of whether the assumptions inherent in these different forms lead also to some noticeable discrepancies in the evaluation of the present EOS data for indium, which cover a reasonably wide range in compression. On the other hand, more recently, two other (second-order) EOS forms were proposed[4,15] with the correct asymptotic behavior at very strong compression. While the form

$$\text{H02: } p=3K_0x^{-5}(1-x)\exp[C_{02}(1-x)] ,$$
$$\text{with } C_{02}=\tfrac{3}{2}(K_0'-3)$$

may be considered just as a small modification with respect to the form MV2, using, however, the correct asymptotic exponent 5 for the term x^{-n}, the best asymptotic fit is obtained with the form

$$\text{H12: } p=3K_0x^{-5}(1-x)\exp[C_{10}(1-x)+xC_{12}(1-x)] ,$$

with $C_{10}=-\ln(3K_0/p_{\mathrm{FG}_0})$ and $C_{12}=\frac{3}{2}(K_0'-3)-C_{10}$. Thereby $p_{\mathrm{FG}_0}=a_{\mathrm{FG}}(Z/V_0)^{5/3}$ with $a_{\mathrm{FG}}=23.37$ MPa nm^5 represents the pressure of a free-electron gas (Fermi gas) with an electron density of Z electrons in the volume V_0 for the solid at ambient conditions. It has been discussed previously[15,23] that EOS data can be represented very conveniently in different "linearization schemes" to illustrate specific features of these data. Thereby, a close relation can be noticed also between a specific EOS form and the related linearization scheme.[15] The specific linearization scheme with the "generalized stress parameter,"

$$\eta_H=\ln\left[\frac{px^5}{p_{\mathrm{FG}_0}(1-x)}\right] ,$$

is specially suited to represent data for solids under strong compression,[4] since the scaling by the Fermi gas pressure $p_{\mathrm{FG}}=p_{\mathrm{FG}_0}/x^5$ leads to the limiting value of $\eta_H\to 0$ for $x\to 0$ and thus allows for a simple interpolation between this value for ultimate compression and the finite value of $\eta_H=\ln(3K_0/p_{\mathrm{FG}_0})=-C_{10}$ for $x=1$ corresponding to zero pressure. A direct representation of all EOS data for indium in this η_H-x linearization scheme is shown in Fig. 6. In this figure, one can see more clearly differences between the data sets than in Fig. 5. One can notice a deviation of the reduced shock-wave data[3] at low compression (small dots), which may be due to the use of a wrong value for V_0. A new fitting of these data with V_0 as fit parameter and rescaling with this new V_0 results in the data points displayed as small crosses in Fig. 6. The value of this new V_0 is slightly larger than the value from the literature.[14] All further calculations done with this data set are using this new $V_0=0.0264$ nm^3. Drastic deviations are shown by the data of Refs. 17 and 18. These data sets are omitted in the following fits. Figure 7(a) illustrates in similar form the present data together with various fitted curves in the experimental region $0.85\le x\le 1$. For a more detailed discussion of the different EOS forms an extrapolation of all the fitted curves into the region of very strong compression ($x\to 0$) is given in Fig. 7(b), where the divergency becomes obvious. Since the scatter of the present as well as previous data at $x\to 1$ becomes very large, the limiting value η_{H_0} using the isothermal value for K_0 from ultrasonic measurements[24,25] is also included in these diagrams. The fitted curves, corresponding to the data given in the first block of Table I, seem to deviate from each other only marginally within the experimental region $0.85\le x\le 1$, however, due to the different curvatures inherent in these second-order fits, slight differences for the corresponding values at $x=1$ can be noticed also in this diagram according to the differences in the parameters given in Table I. Significant differences between the curves H02 and H12 cannot be noticed in this limited range of x and the agreement with the ultrasonic values appears to be very good for any of these curves. However, if one looks at the η_H-x plot for the extended region in $0<x<1$,

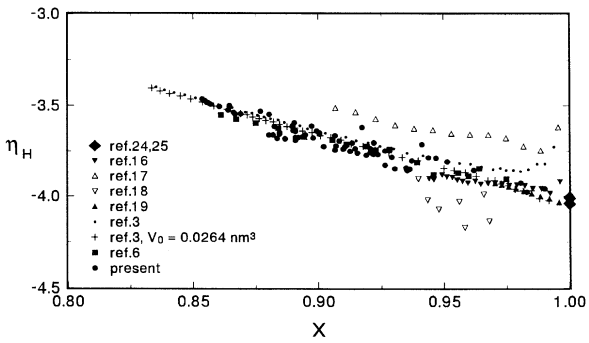

FIG. 6. Different data sets (present and from the literature) represented in η_H-x scaling. The small dots refer to shock-wave data from Ref. 3 and the crosses represent the same data after rescaling with $V_0=0.0264$ nm^3.

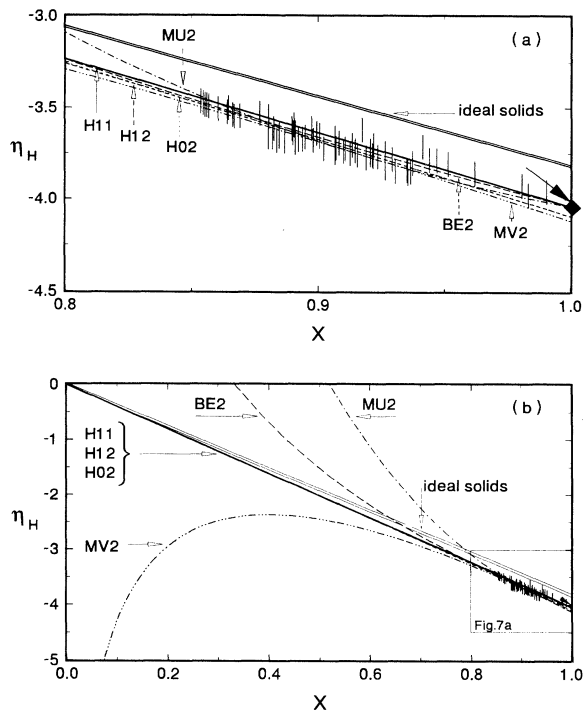

FIG. 7. Representation of the present EOS data with different fitted EOS forms denoted by MU2, BE2, MV2, H02, and H12 using the scales stress parameter η_H and the scaled length parameter x (for details see text). The values for η_H at ambient pressure from ultrasonic data (Table I) are represented by the diamond (Ref. 24) and the arrow (Ref. 25), respectively, whereby the direction of the arrow corresponds to the ultrasonic value for K_0'. The extended diagram for extreme compression ($0 \leq x \leq 1$) includes also the EOS for "ideal solids" as a thin double line.

drastic divergences with respect to the limiting behavior ($\eta_H \rightarrow 0$) can be noticed for all the previously used forms (MU2, BE2, MV2). It is also seen that the different curvatures inherent in these forms are responsible for the (slight) differences in the values for K_0 derived in the fits of these forms to the present data (Table I, first block, and Fig. 7). The deviation between the linear (two-parameter) form H02 and the (more reasonable) nonlinear (two-parameter) form H12 is very small even at very strong compression and suggests that already the one parameter form H11 with $C_{12}=0$ and the corresponding correlation for $K_0'=3-(\frac{2}{3})\ln(3K_0/p_{\mathrm{FG}_0})$ related to the slope of this straight line represents the data perfectly. Thus, the one-parameter first-order EOS form H11 derived from H12 with $C_{12}=0$ and with K_0' coupled to K_0/p_{FG_0} as discussed before fits all the present data perfectly even if just the ultrasonic value for K_0 is used without any free parameter left for fitting, while all the other (second-order) forms (MU2, BE2, MV2) would require still fitting of their values for K_0' even if the value for K_0 is used from ultrasonic measurements. One may now wonder how it comes that one special one-parameter form (H11) can fit the experimental data equally well or even better (see Table I) than other two-parameter forms (MU2, BE2, MV2) more commonly in use. Due to the correct limiting behavior for $x \rightarrow 0$ incorporated into H11, however, more physically reasonable assumptions are incorporated into H11. Therefore, H11 is very appropriate for the representation of EOS data for "simple" solids. Special solids with special electronic "transitions" under pressure can show, however, significant deviations from this simple behavior (H11), as discussed just recently with respect to the special behavior of the regular rare-earth metals[26] or with respect to thorium under strong compression.[27]

In any case, it can be noticed in Fig. 7 that the (best fitting) EOS for indium also comes rather close to the double line which represents the general behavior of "ideal" solids just discussed in a recent publication.[4] At this point, the critical comparison of the present data with previous results represented in Table I needs some further discussion. Since the comparison of the fits with different EOS forms for the present data, either with free or fixed (best ultrasonic) values for K_0 in the first and second blocks of Table I, shows in general a slight superiority in the standard deviations σ_V for H12 (or at least no significant deterioration with respect to any other form), the fit of the previous data is therefore performed only with H12. If one compares then the numerical values and statistical errors for the parameters K_0 and K_0', one can notice that some of the values are in fact incompatible with each other within the given statistical errors, and these inconsistencies become even more evident when all the experimental data are compared, as shown in the third section of Table I. However, if one takes into account that the values of the fitted parameters K_0 and K_0' are strongly (anti-) correlated, as shown by the data for the correlation coefficients $-\epsilon \rightarrow 1$, one can notice in the representation of the corresponding error ellipsoids illustrated in Fig. 8 that only the earliest x-ray-diffraction data[17] are inconsistent with the other volumetric, shock-wave, and x-ray results. The value for K_0' from the high-pressure ultrasonic study[25] may be affected by a larger error than given in the original work, since this ultrasonic high-pressure study did not use any pressure transmitting fluid to avoid possible systematic errors due to nonhydrostatic stresses. Whereas the former discrepancy could be resolved possibly by the use of a revised pressure scale in the evaluation of the early x-ray data,[17] a difference between ultrasonic and volumetric measurements could be expected (after the standard correction from adiabatic to isothermal conditions), at least in principle, for noncubic materials such as indium in polycrystalline form, where different elastic-plastic boundary conditions between the individual grains in the compacted samples can lead to a distinction between two limiting cases[28,29]—the (stress-free) Reuss case for ideal slipping of the grains and the (strain-free) Voigt case for ideal sticking. What is most striking in Fig. 8 (as well as in Fig. 9, to be discussed later) is, however, the fact that the correlation of K_0 and K_0' incorporated in H11 by the assumption of $C_{12}=0$ and represented in Figs. 8 and 9 by the dotted curve (H11) cuts through all ellipsoids (besides the erroneous one of Ref. 17) just in the region of largest overlap. Thus the

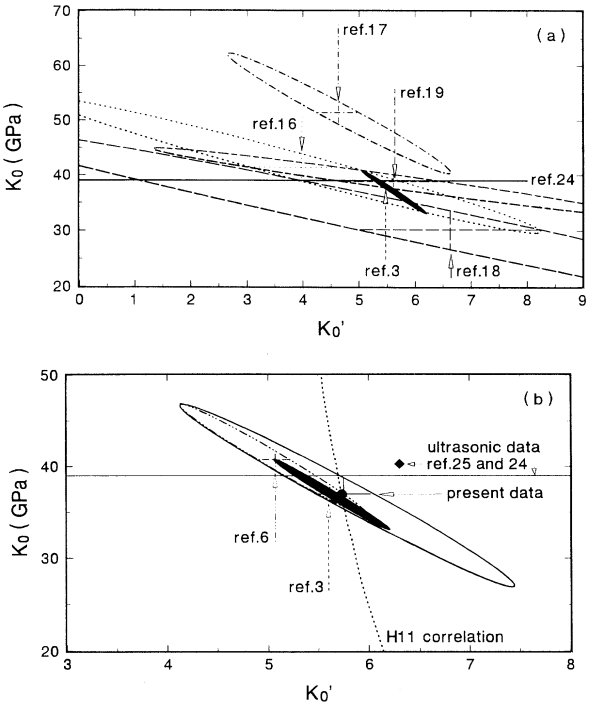

FIG. 8. Error ellipsoids for K_0 and K_0' for different data sets from the literature. For more clarity this figure is divided in two parts: (a) shows the error ellipsoids for earlier static measurements (Ref. 16,18,17, and 19) and shock-wave results (Ref. 3). For comparison, the (isothermal) values from ultrasonic measurements are indicated by the thin line (Ref. 24). The ellipsoid for the present data is compared with the ellipsoid for the data of Ref. 6, the ultrasonic data (Refs. 24 and 25) and the shock-wave results (Ref. 3).

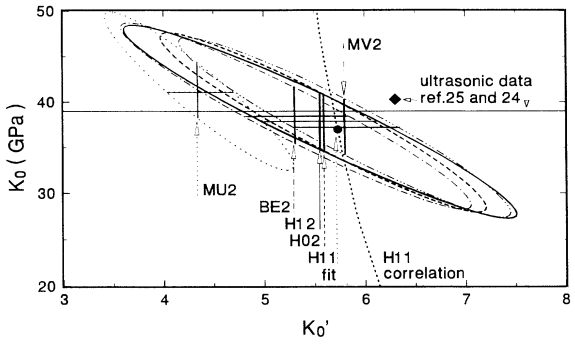

FIG. 9. Error ellipsoids representing the correlations in the values for the best fitted parameters K_0 and K_0' as derived from the present data with the different EOS forms. The contractions of the error ellipsoids by the use of the one-parameter form H11 is illustrated by the solid circle. The dotted line represents the correlation between K_0 and K_0' inherent in the form H11 as discussed in the text. Values from ultrasonic measurements (Refs. 24 and 25) are added.

form H11 would reduce the "statistical" error drastically for any of these data sets and shift the best fitting values into a region of largest consent. However, a significant difference with respect to the (high-pressure) ultrasonic data[25] seems to remain in any case.

To elucidate the origin of this discrepancy further, all the volumetric, x-ray, and shock-wave data are fitted finally together with the different EOS forms previously discussed. The results of these fits are represented in numerical form in Table I in the fourth block and in Fig. 9 by the corresponding error ellipsoids. Here, the distinctly different result of a fit with MU2 is most prominent and can be traced back to the unreasonable assumption $K_0''=0$ inherent in MU2. While the ellipsoids for H02 and H12 are both centered between the ellipsoids for BE2 and MV2, the small but significant discrepancy to the ultrasonic high-pressure measurement[25] seems to remain, with H11 intersecting the other ultrasonic data[24] about halfway with respect to the best value one would obtain for K_0' from all the EOS data with K_0 fixed to the ultrasonic value.[24] If one takes this remaining discrepancy seriously—and further ultrasonic high-pressure studies may have to be performed to settle this question—one could consider this discrepancy as an experimental proof for the difference between volumetric values more closely related to the Voigt limit and ultrasonic values related to the Reuss limit. Since an estimate of the difference between the Voigt and Reuss limits[28] leads to much smaller differences, one may come to the conclusion that nonhydrostatic stresses affected indeed the value of K_0' in the ultrasonic high-pressure study.[25] If, on the other hand, precise ultrasonic measurements for K_0' would become available, K_0'' would have to be used as the next higher-order parameter in any of the higher-order forms (BE3, MV3, or H13) which would result in Fig. 9 in a third dimension for K_0'' related to the next higher-order fitting parameter. This third dimension would lead to oblique three-dimensional error ellipsoids, whose central plain would cut the perpendicular axis above the ultrasonic data point[25] at the best fitting value for K_0''. Due to the present experimental uncertainties, this procedure can serve right now only for an estimate of the possible *absolute* uncertainties in the parameters K_0, K_0', K_0'' in addition to the *restricted errors* given in Table I and Fig. 9 and derived under the assumption of "simple" EOS forms with one or two free parameters for the fit of the data. The specific assumptions correspond thereby to specific correlations for the higher-order parameters like K_0'' discussed in a previous paper.[5]

Finally, it should be stressed that electronic and structural anomalies cannot completely be ruled out as possible effects leading to significant deviations from the smooth interpolation at stronger compression given by the form H12. However, a rough estimation of these possible uncertainties can be made under the assumption that these anomalies should be related at the most to energy differences of the order of the energy E_0, which is roughly given by $K_0V_0/4.5$ (as, for instance, implied by the form BE2). Thus, one would estimate that any deviations from the most "regular" behavior in terms of a volume difference ΔV at a given pressure p should be smaller than $|p\Delta V| \leq E_0 \approx K_0V_0/4.5$, or in other words, $|\Delta V/V_0| \leq K_0/(4.5p)$. With experimental uncertainties

of roughly 1% for the volume data, it would be difficult, therefore, to observe any anomalies at pressures $p \geq 25K_0$, which corresponds (with the form H12) typically to 50% volume compression. Thus, strong deviations from the smooth interpolation form H12 are expected only at intermediate compressions ($V \geq 0.5V_0$), with the exception of hydrogen and the rare gas solids, since the extremely small cohesive energies of these elements could result in significant deviations from this "normal" behavior at even stronger compressions.

ACKNOWLEDGMENT

Financial support by the German Ministry of Research and Technology (BMFT) under contract No. 05 440 AXI4 is gratefully acknowledged.

[1]A. Jayaraman, Rev. Sci. Instrum. **57**, 1013 (1986).
[2]Y. K. Vohra, S. J. Duclos, K. E. Brister, and A. L. Ruoff, Rev. Sci. Instrum. **58**, (1987).
[3]G. C. Kennedy, and R. N. Keeler, in *American Institute of Physics Handbook,* 3rd ed. (McGraw-Hill, New York, 1972), p. 4-38.
[4]W. B. Holzapfel, *Molecular Systems Under High Pressure,* edited by R. Pucci and G. Piccitto (Elsevier, Amsterdam, 1991), p. 61.
[5]W. B. Holzapfel, Europhys. Lett. **16**, 67 (1991).
[6]K. Takemura, Phys. Rev. B **44**, 545 (1991).
[7]G. Huber, K. Syassen, and W. B. Holzapfel, Phys. Rev. B **15**, 5123 (1977).
[8]K. Syassen and W. B. Holzapfel, J. Appl. Phys. **49**, 4427 (1978).
[9]R. A. Forman, G. J. Piermarini, J. D. Barnett, and S. Block, Science **176**, 284 (1972).
[10]M. K. Mao, P. M. Bell, J. W. Sharner, and J. D. Steinberg, J. Appl. Phys. **52**, 4572 (1977).
[11]W. B. Holzapfel and W. May, Adv. Earth Planet. Sci. **12**, 73 (1982).
[12]W. A. Grosshans, E. F. Düsing, and W. B. Holzapfel, High Temp. High Pressures **16**, 539 (1984).
[13]O. Schulte, A. Nikolaenko, and W. B. Holzapfel, High Pressure Res. **6**, 169 (1991).
[14]J. Donohue, *The Structure of the Elements* (Wiley, New York, 1974).
[15]W. B. Holzapfel, High Pressure Res. **7**, 290 (1991).
[16]P. W. Bridgman, Am. Acad. Arts Sci. **76**, 1 (1945).
[17]R. W. Vaughan and H. G. Drickamer, J. Chem. Phys. Solids **26**, 1549 (1965).
[18]L. F. Vereshchagin, S. S. Kabalkina, and Z. V. Troitskaya, Dok. Akad. Nauk SSSR **158**, 1061 (1964) [Sov. Phys. Dok. **9**, 894 (1965)].
[19]S. N. Vaidya and G. C. Kennedy, J. Phys. Chem. Solids **31**, 2329 (1970).
[20]F. D. Murnaghan, *Finite Deformation of an Elastic Solid* (Wiley, New York, 1951).
[21]F. Birch, Phys. Rev. **71**, 809 (1947).
[22]P. Vinet, J. R. Smith, J. Ferrante, and J. H. Rose, Phys. Rev. B **35**, 1945 (1987).
[23]R. Jeanloz, Phys. Rev. B **38**, 805 (1988).
[24]D. R. Winder and C. S. Smith, J. Phys. Chem. Solids **4**, 128 (1958).
[25]F. F. Voronov and V. A. Goncharowa, Fiz. Tverd. Tela (Leningrad) **13**, 3719 (1971) [Sov. Phys. Solid State **13**, 3146 (1972)].
[26]W. A. Grosshans and W. B. Holzapfel, Phys. Rev. B **45**, 5171 (1992).
[27]Y. K. Vohra and W. B. Holzapfel, High Pressure Res. (to be published).
[28]G. Simmons and H. Wang, *Single Crystals Elastic Constants and Calculated Aggregate Properties* (MIT Press, Cambridge, MA, 1971).
[29]E. Schreiber, O. L. Anderson, and N. Soga, *Elastic Constants and Their Measurement* (McGraw-Hill, New York, 1973).